Journal of Alloys and Compounds 509 (2011) 2320–2325

Contents lists available at ScienceDirect

Journal of Alloys and Compounds

journal homepage: www.elsevier.com/locate/jallcom

Study of the structure, magnetic properties and free energy of the three phase composites $La_{0.7-y-z}Sr_{0.3-x}Mn_{1-\delta/3}O_{3-\delta}/(La_2O_3)_{y/2}/(La(OH)_3)_z$

S.P. Liu, G.D. Tang*, Z.Z. Li, W.H. Qi, D.H. Ji, Y.F. Li, W. Chen, D.L. Hou

Hebei Advanced Thin Films Laboratory, Department of Physics, Hebei Normal University, Shijiazhuang City 050016, People's Republic of China

ARTICLE INFO

Article history:
Received 9 May 2010
Received in revised form 31 October 2010
Accepted 2 November 2010
Available online 11 November 2010

Keywords:
Manganites
Crystal structure
Curie temperature
Free energy

ABSTRACT

The structural and magnetic properties and the free energy of manganites with the nominal composition $La_{0.7}Sr_{0.3-x}MnO_{3-\delta}$ ($0 \le x \le 0.10$) have been investigated. X-ray diffraction patterns indicate that the materials possess three phases with the $R\bar{3}c$ perovskite being the dominant phase, La_2O_3 being the second phase and $La(OH)_3$ being the third phase. Due to the samples were prepared using a solid-state reaction method with the highest heat treatment temperature being 1173 K, we assume that there were no vacancies in the perovskite phase. These materials can be represented as $La_{0.7-y-z}Sr_{0.3-x}Mn_{1-\delta/3}O_{3-\delta}/(La_2O_3)_{y/2}/(La(OH)_3)_z$, with $\delta = 3(x+y+z)$. Magnetization measurements showed that the dependence of the Curie temperature T_C on the Mn^{4+} ion content, is similar to that of the typical perovskite manganite $La_{1-x}Sr_xMnO_3$. The paramagnetic–ferromagnetic transition region of the samples is wider than 315 K. We have also calculated the free energy of the perovskite phase, and explained successfully the dependences on the doping level x of the unit cell volume in the perovskite phase.

1. Introduction

Colossal magnetoresistance (CMR) materials [1–4] with the general formula $Ln_{1-x}M_xMnO_3$, where Ln is the lanthanide cation and M is usually an alkaline-earth cation, have attracted much attention because of their potential applications in magnetic sensors, data storage, and other applications, such as the cathodes of the solid oxide fuel cells [5–7] (SOFCs) and microwave dielectric materials [8–10]. These materials possess an ABO_3 perovskite structure. Zener proposed that the spin structure and the electronic properties of these compounds are correlated via the double exchange (DE) mechanism. According to this picture, in the configuration Mn^{3+}–O^{2-}–Mn^{4+}, the easy simultaneous transfer of an electron (DE carrier) from Mn^{3+} to O^{2-} to Mn^{4+}, causes at the same time a high electrical conductivity and, by the tendency of the traveling electron to retain its spin orientation, a parallel orientation of the magnetic moments of the Mn^{3+} and Mn^{4+} ions [11,1,2].

Previous study in our group has demonstrated methods of phase analysis and calculating the various ion contents of perovskite phase in lanthanum deficiency in $La_{0.7-x}Sr_{0.3}MnO_3$ composition samples with Mn_3O_4 second phase [12]. In this paper, we investigate the self-doped perovskite manganites with nominal composition $La_{0.7}Sr_{0.3-x}MnO_3$ prepared by a solid-state reaction method with the highest heat treatment temperature being 1173 K. It is found that these materials can be represented as $La_{0.7-y-z}Sr_{0.3-x}Mn_{1-\delta/3}O_{3-\delta}/(La_2O_3)_{y/2}/(La(OH)_3)_z$, with $\delta = 3(x+y+z)$.

2. Experimental details

Polycrystalline samples with the nominal composition $La_{0.7}Sr_{0.3-x}MnO_3$ ($x = 0$, 0.05, 0.075, and 0.1) were synthesized using the solid-state reaction method. The starting materials were La_2O_3, $SrCO_3$, and MnO_2 powders. The La_2O_3 was fired in air at 1073 K for 3 h before use in order to ensure that is dry. The starting materials were intimately mixed in an agate mortar, grinding for 3 h, and heated in air at temperatures up to 1173 K for 24 h, followed by furnace cooling. The samples studied in this work were obtained after regrinding.

Phase identification of the samples was performed by X-ray diffraction (XRD) with an X'pert Pro diffractometer using Cu K_α radiation. The data were collected in the 2θ range 20–120° with a step size of 0.0167°. The magnetization measurements were carried out using a Quantum Design Physical Property Measurement System (PPMS), in the temperature range 5–400 K. The temperature at which the dM/dT curve tends to zero with increasing temperature indicates the Curie temperature (T_C). The Curie temperature measurements were performed at an applied field of 0.05 T. In order to facilitate the discussion, we label the samples with nominal compositions $La_{0.7}Sr_{0.3-x}MnO_3$ ($x = 0.00$, 0.05, 0.075, and 0.10) as N1, N2, N3, and N4, respectively.

3. Results and discussion

3.1. X-ray diffraction analyses

Fig. 1 shows the X-ray diffraction patterns for the samples. It can be seen that all the samples contain three phases with the $R\bar{3}c$

* Corresponding author.
E-mail address: tanggd@mail.hebtu.edu.cn (G.D. Tang).

0925-8388/$ – see front matter © 2010 Elsevier B.V. All rights reserved.
doi:10.1016/j.jallcom.2010.11.009

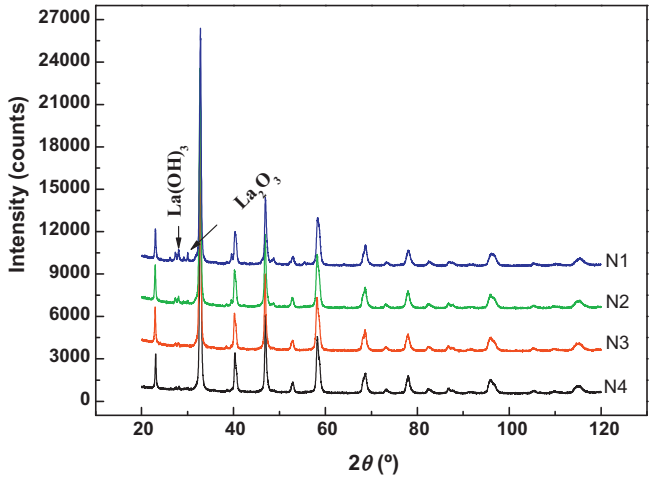

Fig. 1. XRD diffraction patterns of the samples with nominal composition $La_{0.7}Sr_{0.3-x}MnO_{3-\delta}$. The main diffraction peaks of the La_2O_3 phase and $La(OH)_3$ phase are marked by the symbol "↓".

perovskite being the dominant phase, La_2O_3 being the second phase and $La(OH)_3$ being the third phase. The main diffraction peaks of the La_2O_3 phase and $La(OH)_3$ phase are marked by the symbol "↓". The diffraction peak positions of the three phases, according to the Rietveld powder diffraction profile fitting software (see below), are shown in Fig. 2. The upper series belongs to the perovskite phase, the middle series to the La_2O_3 phase and the lower series to the $La(OH)_3$ phase. The reason for the appearance of the impurities, La_2O_3 and $La(OH)_3$, is that the melting point of MnO_2 is only 808 K, which is far lower than other starting materials (being higher than 1770 K), so that it is easy to escape from the raw materials during the samples preparation process.

By using the X'Pert HighScore Plus software to analyze the XRD patterns, the volume averaged crystallite diameters of the perovskite phase in the samples can be estimated. They were found to be 32, 38, 37, and 35 nm for samples N1, N2, N3, and N4, respectively. These values indicate that these samples were nanocrystalline composite materials.

Quantitative analyses of the three phases were performed using the main diffraction peak intensity ratios obtained using the X'Pert HighScore Plus software. We use the symbols "u" and "v" to designate the mass ratios of the La_2O_3 and $La(OH)_3$ phases to the perovskite phase, respectively. According to X-ray diffraction theory we then have

$$u = \frac{W_{LO}}{W_P} = \frac{I_{LO}/K_{LO}}{I_P/K_P} = \frac{5.44}{8.20}\frac{I_{LO}}{I_P}, \quad v = \frac{W_{LH}}{W_P} = \frac{I_{LH}/K_{LH}}{I_P/K_P} = \frac{5.44}{6.86}\frac{I_{LH}}{I_P}, \tag{1}$$

where W_{LO}, W_{LH} and W_P are the masses of the La_2O_3 phase, $La(OH)_3$ phase and the perovskite phase respectively; I_{LO}, I_{LH} and I_P are the main diffraction peak intensities of the La_2O_3, $La(OH)_3$ and perovskite phases, respectively; K_{LO}, K_{LH} and K_P, with the values 8.20, 6.86 and 5.44, respectively, come from the *RIR* values for La_2O_3, $La(OH)_3$ and perovskite $La_{0.7}Sr_{0.3}MnO_3$ on the ICDD standard cards 01-074-1144, 01-083-2034 and 01-089-4461. They each represent

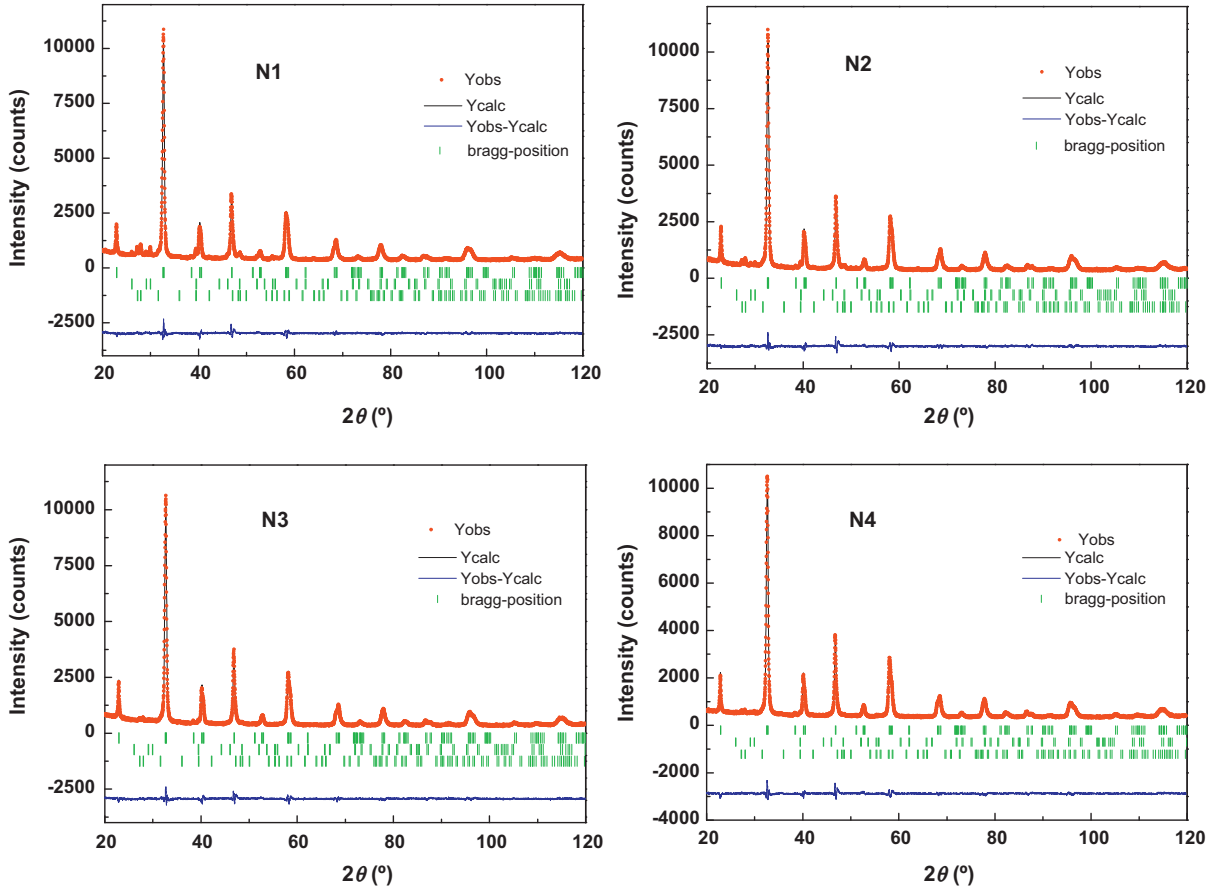

Fig. 2. The Rietveld fitted results for the XRD diffraction data of the samples with the nominal composition $La_{0.7}Sr_{0.3-x}MnO_{3-\delta}$ (x = 0.00, 0.05, 0.075, and 0.10, corresponding to samples N1, N2, N3, and N4). Here "•" represents the experimental intensity Y_{obs}. The bottom line shows the difference $Y_{obs} - Y_{cal}$ between the experimental and fitted curve. The symbol "|" represents the diffraction peak positions of the three phases. The upper, middle and lower series belong to the perovskite. La_2O_3 and $La(OH)_3$ phases, respectively.

Table 1
The XRD main peak intensities I_P, I_{LO} and I_{LH} of the perovskite phase, La_2O_3 and $La(OH)_3$ phases in the samples with a nominal composition $La_{0.7}Sr_{0.3-x}MnO_{3-\delta}$. The parameters c_{LO}, c_{LH}, y, z and molar content of the perovskite phase M.

No.	x	I_P	I_{LO}	I_{LH}	c_{LO}	c_{LH}	y	z	M
N1	0.000	16276.83	569.30	923.48	5.23567	10.15191	0.02961	0.04924	0.92115
N2	0.050	16472.25	196.92	490.63	1.79383	5.34235	0.01007	0.02572	0.91421
N3	0.075	16011.43	52.59	243.06	0.49348	2.72621	0.00275	0.01305	0.90919
N4	0.100	16041.10	93.62	166.32	0.87365	1.85520	0.00475	0.00866	0.88658

the ratio of the main diffraction peak intensity of the compound in question to that of α-Al_2O_3 when the mass ratio is 1:1. Because there are different values of K_P for the perovskite phase as it occurs in the samples and for $La_{0.7}Sr_{0.3}MnO_3$, the value of K_P used in this expression should be taken as inversely proportional to the density of the samples. Eq. (1) can then be rewritten as

$$u = \frac{W_{LO}}{W_P} = 0.10037\frac{I_{LO}}{I_P}\frac{5.44}{8.20}\frac{d_0V_C}{m_P}, \quad v = \frac{W_{LH}}{W_P} = 0.10037\frac{I_{LH}}{I_P}\frac{5.44}{6.86}\frac{d_0V_C}{m_P}, \tag{2}$$

where m_P and V_C are the molar mass and the unit cell volume of the perovskite phase in our samples, expressed in units of grams (g) and Å^3, respectively. Finally, d_0 is the density of the standard $La_{0.7}Sr_{0.3}MnO_3$ material. Setting

$$c_{LO} = 0.10037\frac{5.44}{8.20}\frac{I_{LO}}{I_P}d_0V_C, \quad c_{LH} = 0.10037\frac{5.44}{6.86}\frac{I_{LH}}{I_P}d_0V_C, \tag{3}$$

then

$$\frac{W_{LO}}{W_P} = \frac{c_{LO}}{m_P} \quad \text{and} \quad \frac{W_{LH}}{W_P} = \frac{c_{LH}}{m_P}. \tag{4}$$

We next designate the molar fractions of La_2O_3 as $y/2$ and $La(OH)_3$ as z. We assume that the missing molar content of MnO_2 is equal to the sum of molar content of La_2O_3 and $La(OH)_3$ plus the doping level x.

Due to the samples were prepared using a solid-state reaction method with the highest heat treatment temperature being 1173 K, we assume that there were no vacancies in the perovskite phase. Therefore the molar content of Mn ions in the perovskite phase is $M = 1-x-y-z$. The molar content of the perovskite phase is then $(0.7-y-z+0.3-x+1-x-z-y)/2 = 1-x-y-z$, and the oxygen molar content is $3(1-x-y-z)$. Note that the molar content of the Mn ions is equal to the molar content of the perovskite phase. The perovskite phase in the samples can therefore be written as $La_{0.7-y-z}Sr_{0.3-x}Mn_{1-\delta/3}O_{3-\delta}$, with $\delta = 3(x+y+z)$. Following our earlier work [12,13], we have the various ion contents

$$L = 0.7-y-z, \quad S = 0.3-x, \quad M_3 = 0.7-y-z, \quad M_4 = 0.3-x, \quad O_2 = 3(1-x-y-z), \tag{5}$$

where L, S, M_3, M_4, and O_2 represent the molar contents of La^{3+}, Sr^{2+}, Mn^{3+}, Mn^{4+} and O^{2+} ions, respectively. Therefore, we can represent the perovskite phase in our samples as $La_{0.7-y-z}{}^{3+}Sr_{0.3-x}{}^{2+}Mn_{0.7-y-z}{}^{3+}Mn_{0.3-x}{}^{4+}O_{3(1-x-y-z)}{}^{2-}$.

Table 2
The molar contents L, S, M_3, M_4, and O_2 of La^{3+}, Sr^{2+}, Mn^{3+}, Mn^{4+} and O^{2-} ions of the perovskite phase in the samples, and the Mn^{4+} ion content ratio, R_{M4}, at the B site.

No.	L	S	M_3	M_4	O_2	R_{M4}
N1	0.62115	0.300	0.62115	0.300	2.76346	0.32568
N2	0.66421	0.250	0.66421	0.250	2.74264	0.27346
N3	0.68419	0.225	0.68419	0.225	2.72758	0.24747
N4	0.68658	0.200	0.68658	0.200	2.65975	0.22558

The mass ratios of the La_2O_3 phase and $La(OH)_3$ phase to the perovskite phase are

$$\frac{W_{LO}}{W_P} = \frac{(y/2)m_{LO}}{(1-x-y-z)m_P}, \quad \frac{W_{LH}}{W_P} = \frac{zm_{LH}}{(1-x-y-z)m_P}, \tag{6}$$

where the molar masses of the La_2O_3 phase and the $La(OH)_3$ phase are, $m_{LO} = 325.809$ g and $m_{LH} = 189.906$ g. From above Eqs. (4) and (6), we then have,

$$y = \frac{(1-x)\times 189.906c_{LO}}{30936.541977 + 189.906c_{LO} + 162.9045c_{LH}}, \quad z = \frac{(1-x-y)c_{LH}}{189.906 + c_{LH}}. \tag{7}$$

Using Eqs. (3), (7) and the main peak intensity ratios of the three phases, we can obtain the parameter y and z. Table 1 lists the main peak intensities I_P, I_{LO}, and I_{LH} of the perovskite, the La_2O_3 and the $La(OH)_3$ phases, the parameters c_{LO}, c_{LH}, y, z and the molar content M of the perovskite phase in the samples. Note again that M is also equal to the molar content of Mn ions in the perovskite phase as shown above.

The contents of the various ions as calculated using Eqs. (5) and (7), are shown in Table 2. In Table 2, R_{M4} which represents the Mn^{4+} ion content ratio at the B site of the ABO_3 structure, is defined by

$$R_{M4} = \frac{M_4}{(M_3+M_4)}. \tag{8}$$

For convenience of interpretation, we also show in Table 3, the same ion contents normalized so that the O^{2-} content is 3, as is appropriate for the standard ABO_3 structure $(La_{0.7-y-z}Sr_{0.3-x})_{1/(1-x-y-z)}MnO_3$.

Using directly the contents of the various ions in Table 3, the XRD diffraction data were fitted using the Rietveld powder diffraction profile fitting technique [14]. In the fitting process, the contents of the various ions were not changed. The three equivalent positions (6a, 6b, and 18e) in the rhombohedral unit cell are occupied by 6 (La^{3+}, Sr^{2+}), 6 (Mn^{3+}, Mn^{4+}), and 18 O^{2-}, respectively. The fitted results are shown in Fig. 2 and Table 4. It may be seen that the

Table 3
The molar contents L, S, M_3, M_4, and O_2 of La^{3+}, Sr^{2+}, Mn^{3+}, Mn^{4+} and O^{2-} ions, the Mn^{4+} ion content ratio R_{M4}, at the B site, and molar mass m_P of the perovskite phase in the samples when the contents of the O^{2-} ions have been normalized to 3. The experimental moments σ_{SE} at 10 K under 2 T applied magnetic field, and theoritical moments σ_{SC} by the $Mn^{3+}$and Mn^{4+} content per molar perovskite phase in the samples.

No.	L	S	M_3	M_4	O_2	R_{M4}	m_P	σ_{SE} (μ_B)	σ_{SC} (μ_B)
N1	0.67432	0.32568	0.67432	0.32568	3	0.32568	225.14	3.47160	3.67432
N2	0.72654	0.27346	0.72654	0.27346	3	0.27346	227.82	3.48227	3.72654
N3	0.75253	0.24747	0.75253	0.24747	3	0.24747	229.15	3.48476	3.75253
N4	0.77442	0.22558	0.77442	0.22558	3	0.22558	230.27	3.51968	3.77442

Table 4
The refined parameters for the rhombohedral perovskite phase in samples with the nominal composition $La_{0.7}Sr_{0.3-x}MnO_{3-\delta}$, the atomic coordinate at A, B and O site, calculated Mn–O bond lengths d and Mn–O–Mn bond angles Θ, the profile factor R_p, the weighted profile factor R_{wp}, goodness of fit indicator s. Where S.G. is the space group, Z is the formular number per rhombohedral unit cell, a and c are lattice parameters, and V is the cell volume.

Samples	N1	N2	N3	N4
S.G.	$R\bar{3}c$	$R\bar{3}c$	$R\bar{3}c$	$R\bar{3}c$
Z	6	6	6	6
a (Å)	5.492(6)	5.499(0)	5.501(9)	5.506(5)
c (Å)	13.346(2)	13.347(7)	13.350(2)	13.362(2)
V (Å^3)	348.7(0)	349.5(4)	349.9(8)	350.8(8)
A($La^{3+}Sr^{2+}$)				
x	0	0	0	0
y	0	0	0	0
z	0.25	0.25	0.25	0.25
B($Mn^{3+}Mn^{4+}$)				
x	0	0	0	0
y	0	0	0	0
z	0	0	0	0
O				
x	0.468(3)	0.464(0)	0.462(2)	0.461(9)
y	0	0	0	0
z	0.25	0.25	0.25	0.25
d (Å)	1.944(5)	1.948(3)	1.950(2)	1.952(5)
Θ (°)	169.7(5)	168.3(5)	167.7(7)	167.4(0)
R_p (%)	3.78	3.80	3.89	4.15
R_{wp} (%)	4.79	4.90	4.92	5.25
s	1.16	1.19	1.18	1.24

final fitting parameters, profile factor R_p, weighted profile factor R_{wp} and goodness of fit indicator s, are satisfactory, indicating that the contents of the various ions calculated by the above method are reasonable. From Table 4, it may be seen that the lattice parameters a and c, the cell volume V, Mn–O bond length d, the Mn–O–Mn bond angle Θ, have all changed significantly.

3.2. Magnetic property analyses

Fig. 3(a) shows curves of the specific magnetization, σ, versus temperature at an applied field of 0.05 T. The curves show that with decreasing temperature, all samples exhibit a paramagnetic to ferromagnetic transition. Fig. 3(b) shows the curves $d\sigma/dT$ versus temperature. The absolute values of $d\sigma/dT$ begin to increase from near zero when $T = T_{CL}$ (taken at $d\sigma/dT = -0.1$), reach a maximum value when $T = T_{CM}$, and decrease to near zero when $T = T_C$ (taken at $d\sigma/dT = -0.1$). With increasing doping level x, the Curie temperature T_C shifts from 372 K for $x = 0$–353 K for $x = 0.1$. The transition region from ferromagnetism to paramagnetism, $\Delta T = T_C - T_{CL}$, is wider than 315 K. The main reason for this wide transition temperature range is that the volume averaged crystallite diameters of the perovskite phase are 32, 38, 37, and 35 nm in samples N1, N2, N3, and N4, respectively. The magnetic ordered temperature of the ion layers in the crystallites increases with decreasing the layer radius, with the result that the average angle between the Mn ionic moments decreases with decreasing the layer radius. We plot in Fig. 4 the relations of the magnetic ordered temperatures T_{CL}, T_{CM}, T_C, and ΔT versus the Mn^{4+} ion content ratio, R_{M4}, at the B site. From Fig. 4 and Table 4, it can be seen that the tendency of the change of the Curie temperature T_C is the same as that of the Mn–O–Mn bond angles Θ, and is contrary to the Mn–O bond length d and unit cell volume V_C. These experimental phenomena can be explained using Zener's double exchange interaction between Mn^{3+} and Mn^{4+} ions [11,1,2].

Curves of the specific magnetization σ versus the applied field for the samples, tested at 300 K and 10 K, are shown in Fig. 5(a) and (b). It can be seen that the coercivity is very small in all our samples. At 10 K, the specific saturation magnetization σ_{SE} of the samples

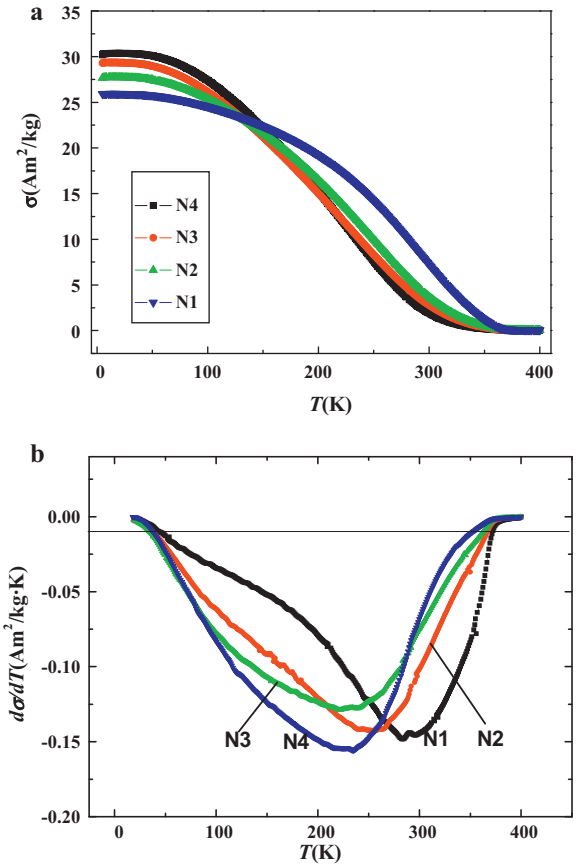

Fig. 3. (a) Curves of the specific magnetization σ of the samples with the nominal composition $La_{0.7}Sr_{0.3-x}MnO_{3-\delta}$ versus temperature at an applied field of 0.05 T, (b) curves of $d\sigma/dT$ versus temperature.

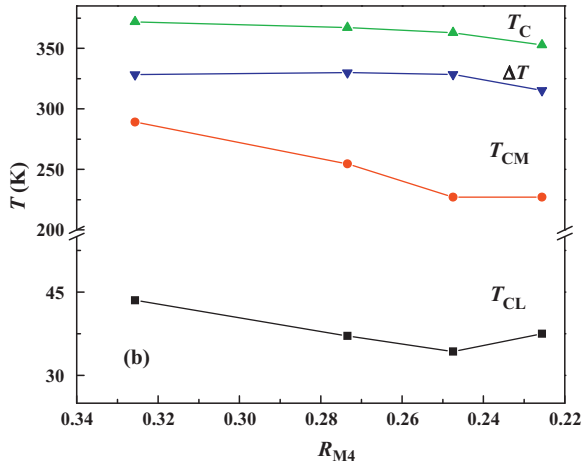

Fig. 4. The R_{M4} dependences of the magnetic ordered temperatures T_{CL}, T_{CM}, T_C, and ΔT.

increases with decreasing Mn^{4+} ion content ratio R_{M4}, which is in agreement with the theoretical values, σ_{SC}, as shown in Table 3. The value of σ_{SE} is about 94% of σ_{SC}, because the volume averaged crystallite diameters of the perovskite phase are between only 32 and 38 nm. At 300 K, the specific magnetization σ does not reach saturation until the applied field is increased to 2 T. The σ(2 T) is trend as a function of R_{M4} is contrary to that of σ_{SE} at 10 K, resulting from the fact that 300 K is obviously higher than the magnetic ordered temperature T_{CM} of the main phase in the perovskite nanocrystallites.

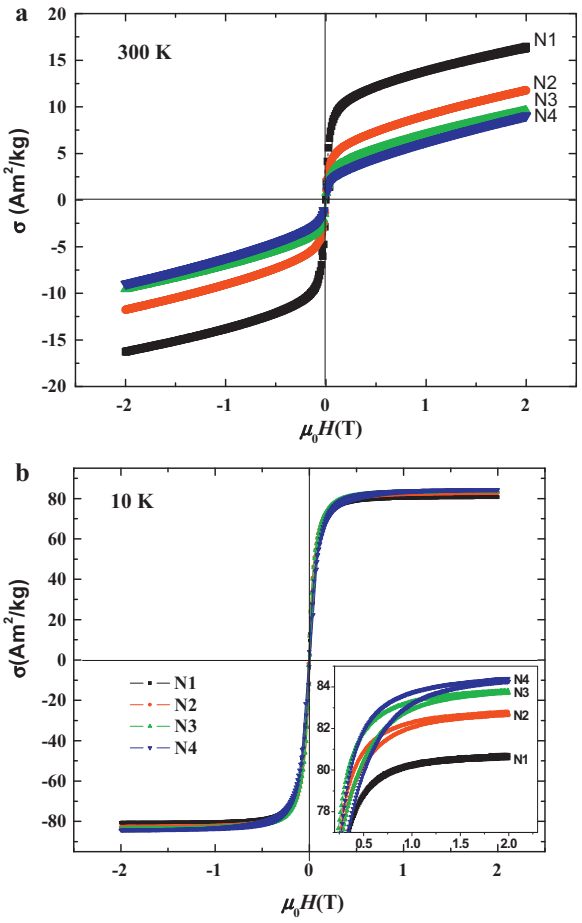

Fig. 5. Curves of the specific magnetization σ of the samples versus the applied field tested at 300 K (a) and 10 K (b).

3.3. Free energy considerations concerning the dependence of the unit cell volume in the perovskite phase on the doping level

From Table 4, it can be seen that the unit cell volume of the perovskite phase in the samples increases with increasing doping level x. This can be explained using the free energy of the unit cell [15,16]. In order to make the discussion of the cell volume more convenient, we transform the rhombohedra perovskite unit cell to the equivalent cubic cell, with lattice constant a_0 (volume $V_0 = a_0^3$), in which there is only one ABO_3 group of atoms. Therefore, the problem of the doping level x dependence of the unit cell volume can be considered in terms of the dependence of the crystal lattice constant a_0 on the doping level. The average free energy per equivalent cubic cell of the perovskite phase can be represented [15] as a sum,

$$F = U - TS = u_C + u_{PR} + u_{TV}, \tag{9}$$

$$u_C = u_\alpha + u_b + u_d = -\frac{q^2}{4\pi\varepsilon_0 a}\left[\alpha + c_b y \cos\left(\frac{\pi T^5}{2T_C^5}\right) + \frac{c_d}{a^2} e^{-E_u/k_B T}\right], \quad (c_b = 0, \quad \text{when} \quad T > T_C), \tag{10}$$

$$u_{PR} = \frac{\alpha q^2}{4\pi\varepsilon_0}\left(\frac{c_{BO}}{(a/2)^i} + \frac{c_{AO}}{(a/\sqrt{2})^j} + \frac{c_{OO}}{(a/\sqrt{2})^m} + \frac{c_{AB}}{(\sqrt{3}a/2)^n}\right), \tag{11}$$

$$u_{TV} = \left(\frac{a}{0.385}\right)^{5/3} \times 9Nk_B T\left(\frac{T}{\theta_D}\right)^3 \int_0^{\theta_D/T} x^2 \ln(1 - e^{-x})dx. \tag{12}$$

Table 5
Parameters used in free energy fitting the doping level dependence of the equivalent cubic cell lattice constant a_0 for the perovskite phase in the samples. The parameters c_d and E_u are the thermal activation energy coefficient of the small polarons, and the thermal activation energy for small polarons, respectively. The Curie temperature T_C, Debye temperature θ_D, the parameters c_b, c_r and Madelung constant α are also listed in the table.

No.	x	T_C (K)	θ_D (K)	α	c_b	c_r	c_d	E_u (eV)
N1	0.00	372	437	45.67	0.3	0.9934	1	0.116
N2	0.05	367	427	45.56	0.3	0.9910	1	0.106
N3	0.075	363	420	45.51	0.3	0.9898	1	0.102
N4	0.10	354	413	45.48	0.3	0.9891	1	0.100

Table 6
The calculated lattice constant a_0 and energies (eV) corresponding to the minimum average free energy F_0 per equivalent cubic cell for the perovskite phase in the samples. Here $u_{\alpha 0}$ is the ionic Coulomb energy, u_{b0} and u_{d0} are the additional energies produced by DE carriers and the thermal activation small polarons, respectively; u_{PR0} is the Pauli repulsion energy, and u_{TV0} is free energy corresponding to the thermal vibration energy of the crystal lattice.

No.	a_0	F_0	$u_{\alpha 0}$	u_{b0}	u_{d0}	u_{PR0}	u_{TV0}
N1	0.38735	−23.0497	−27.1638	−0.04997	−0.04539	4.38619	−0.17664
N2	0.38767	−22.9825	−27.0779	−0.04096	−0.06512	4.38385	−0.18231
N3	0.38784	−22.9534	−27.0384	−0.03626	−0.07532	4.38282	−0.18618
N4	0.38815	−22.9198	−26.9960	−0.03017	−0.08227	4.37975	−0.19016

We can obtain the lattice constant a_0 by minimizing the free energy F with respect to the lattice parameter a. In some ionic semiconductors, the effective unit charge q of the ions is far smaller than the electron charge e. Here we let $q = 0.4e$ [16]. In Eq. (10), u_α is the ionic Coulomb energy; u_b is the additional energy produced by DE carriers, parameter y represents the number of Mn^{3+} and Mn^{4+} ion pairs; u_d is the additional energy produced by small polarons. In Eq. (11), u_{PR} is the Pauli repulsion energy, in which the four terms are the repulsion energies in the O–B bonds, A–O bonds, O–O bonds and A–B bonds, respectively. The parameters $c_{AO} = c_{OO} = 1.00 \times 10^{-6}$, and the parameters $c_{BO} = 3.30 \times 10^{-5}$, $c_{AB} = 1.10 \times 10^{-5}$. The different denominators in the four terms represent the different bond lengths. The indices i, j, m, and n in Eq. (11) are related to the parameters r_k. Here r_k is the weighted average for the O and A or B ions, $r_i = r(Mn^{3+},O^{2-})M_3 + r(Mn^{4+},O^{2-})M_4$, $r_j = r(La^{3+},O^{2-})L + r(Sr^{2+},O^{2-})S$, $r_m = r(O^{2-},O^{2-})$, $r_n = r_i + r_j - r_m$. Here, $r(Mn^{3+},O^{2-})$ is the sum of the Mn^{3+} and O^{2-} effective radii, and similarly for the other parameters $r(\text{ion}, O^{2-})$. The cation contents L, S, M_3 and M_4 come from Table 3. The indices are defined as

$$k = c_r(-1.138 + 3.459 r_k), \quad (k = i, m). \tag{13}$$

$$k = -1.138 + 3.459 r_k, \quad (k = j,\ m). \tag{14}$$

The parameter c_r represents different repulsion power ratios between the shorter r_k (r_i or r_n relating to the Mn ions) and the longer r_k (r_j or r_m relating to non-Mn ions).

In Eq. (12), u_{TV} is the free energy corresponding to thermal vibration of the crystal lattice, θ_D is Debye temperature of the perovskite phase, $N = 5$, representing 5 atoms in every equivalent cubic cell. The parameters c_d and E_u are the thermal activation energy coefficient and the thermal activation energy, respectively, for small polarons. The Curie temperature, T_C, Debye temperature, θ_D [1], Madelung constant, α [16] and the parameters c_b [15] are listed in the Table 5.

Table 6 gives the calculated results: the lattice constant a_0 (nm) of the equivalent cubic cell and the energies (eV) corresponding to the minimum average free energy F_0 per equivalent cubic cell for the perovskite phase in the samples. Here $u_{\alpha 0}$ is the ionic Coulomb energy, u_{b0} and u_{d0} are the additional energies produced by DE carriers and the small polarons by thermal activation, respectively; u_{PR0} is the Pauli repulsion energy, and u_{TV0} is free energy corresponding to the thermal vibration energy of the crystal lattice.

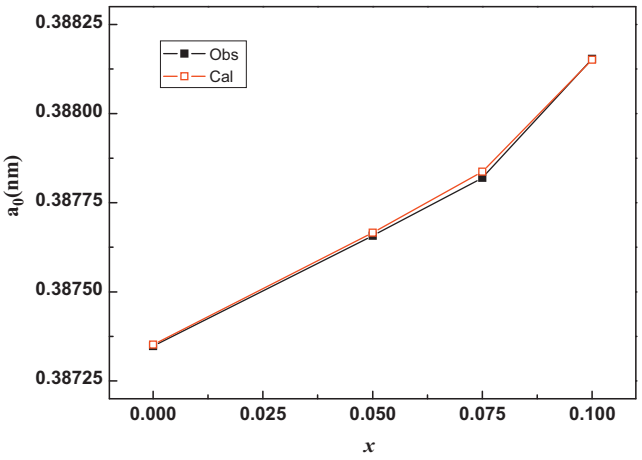

Fig. 6. The dependences of the calculated and experimental equivalent cubic cell lattice constant a_0 in the perovskite manganites on self-doping level x.

Fig. 6 shows the calculated and experimental dependences of the equivalent cubic cell lattice constant a_0 on the Mn^{4+} ion content ratio R_{M4} of the perovskite phase in the samples. It can be seen that the experimental values and the calculated values match very well.

4. Conclusions

We have prepared manganites with the nominal composition $La_{0.7}Sr_{0.3-x}MnO_{3-\delta}$ ($0 \le x \le 0.10$) by a solid-state reaction method with the highest heat treatment temperature being 1173 K. Using XRD analysis, the samples were verified as being three phase composities $La_{0.7-y-z}Sr_{0.3-x}Mn_{1-\delta/3}O_{3-\delta}/(La_2O_3)_{y/2}/(La(OH)_3)_z$, with $\delta = 3(x+y+z)$. We have calculated the ion content ratios at the A, B and O sites of the perovskite phase, and the ratios were shown to be reasonable through Rietveld fitting, analysis of the magnetic property. It was found that the dependences of the Curie temperature T_C on the Mn^{4+} ion content R_{M4} at the B sites, are similar to those of the typical perovskite $La_{1-x}Sr_xMnO_3$. At 10 K, the specific saturation magnetization σ_{SE} of the samples increases with decreasing Mn^{4+} ion content ratio R_{M4}, which is in accord with changes in the theoretical value σ_{SC}. The volume averaged crystallite diameters of the perovskite phase in the samples are between 32 and 38 nm, resulting in the observation that all samples display a very wide paramagnetic–ferromagnetic transition region with decreasing temperature. We calculated the free energy of the perovskite phase, and explained successfully the dependence of the unit cell volume of the perovskite phase on the doping level.

Acknowledgements

This work was supported by the Key Item Science Foundation of Hebei Province No. 08965108D, Natural Science Foundation of Hebei Province No. E2006000168, the National Natural Science Foundation of China Nos. NSF-10774037 and 10074013. The authors wish to thank Dr. Norm Davison for helpful discussion.

References

[1] M.B. Salamon, M. Jaime, Rev. Mod. Phys. 73 (2001) 583.
[2] E. Dagotto, T.i. Hotta, A. Moreo, Phys. Rep. 344 (2001) 1–153.
[3] R. Mahendiran, S.K. Tiwary, A.K. Raychaudhuri, T.V. Ramakrishnan, R. Mahesh, N. Rangavittal, C.N.R. Rao, Phys. Rev. B 53 (1996) 3348–3358.
[4] G.D. Tang, D.L. Hou, W. Chen, X. Zhao, W.H. Qi, Appl. Phys. Lett. 90 (2007) 144101.
[5] B. Lin, S. Wang, H. Liu, K. Xie, H. Ding, M. Liu, G. Meng, J. Alloys Compd. 472 (2009) 556–558.
[6] L. Bi, S. Zhang, B. Lin, S. Fang, C. Xia, W. Liu, J. Alloys Compd. 473 (2009) 48–52.
[7] S. Wang, B. Lin, Y. Chen, X. Liu, G. Meng, J. Alloys Compd. 479 (2009) 764–768.
[8] M. Raama Varma, P. Nisha, P.C. Rajath Varma, J. Alloys Compd. 457 (2008) 422–428.
[9] J. Deng, J. Chen, R. Yu, G. Liu, X. Xing, J. Alloys Compd. 472 (2009) 502–506.
[10] S.-F. Wang, Y.-R. Wang, Y.-C. Wu, Y.-J. Liu, J. Alloys Compd. 480 (2009) 499–504.
[11] C. Zener, Phys. Rev. 82 (1951) 403.
[12] S.P. Liu, G.D. Tang, P. Hao, L.Q. Xu, Y.G. Zhang, W.H. Qi, X. Zhao, D.L. Hou, W. Chen, J. Appl. Phys. 105 (2009) 013905.
[13] G.D. Tang, D.L. Hou, W. Chen, P. Hao, G.H. Liu, S.P. Liu, X.L. Zhang, L.Q. Xu, Appl. Phys. Lett. 91 (2007) 152503.
[14] H.M. Rietveld, J. Appl. Crystallogr. 2 (1969) 65.
[15] G.D. Tang, S.P. Liu, W. Zhao, Y.G. Zhang, D.H. Ji, Y.F. Li, W.H. Qi, W. Chen, D.L. Hou, Appl. Phys. Lett. 95 (2009) 121906.
[16] G.D. Tang, D.L. Hou, Z.Z. Li, X. Zhao, W.H. Qi, S.P. Liu, F.W. Zhao, Appl. Phys. Lett. 89 (2006) 261919.